The Astrophysical Journal, 827:6 (9pp), 2016 August 10 doi:10.3847/0004-637X/827/1/6

AN EMPIRICAL DETERMINATION OF THE INTERGALACTIC BACKGROUND LIGHT FROM UV TO FIR WAVELENGTHS USING FIR DEEP GALAXY SURVEYS AND THE GAMMA-RAY OPACITY OF THE UNIVERSE

Floyd W. Stecker[1,2], Sean T. Scully[3], and Matthew A. Malkan[4]
[1] Astrophysics Science Division, NASA/Goddard Space Flight Center Greenbelt, MD 20771, USA; Floyd.W.Stecker@nasa.gov
[2] Department of Physics and Astronomy, University of California, Los Angeles, USA
[3] Department of Physics, James Madison University Harrisonburg, VA 22807, USA; scullyst@jmu.edu
[4] Department of Physics and Astronomy, University of California, Los Angeles, CA 90095-1547, USA; malkan@astro.ucla.edu
Received 2016 May 4; revised 2016 June 28; accepted 2016 July 2; published 2016 August 3

ABSTRACT

We have previously calculated the intergalactic background light (IBL) as a function of redshift from the Lyman limit in the far-ultraviolet to a wavelength of 5 μm in the near-infrared range, based purely on data from deep galaxy surveys. Here, we use similar methods to determine the mid- and far-infrared IBL from 5 to 850 μm. Our approach enables us to constrain the range of photon densities by determining the uncertainties in observationally determined luminosity densities and spectral gradients. By also including the effect of the 2.7 K cosmic background photons, we determine upper and lower limits on the opacity of the universe to γ-rays up to PeV energies within a 68% confidence band. Our direct results on the IBL are consistent with those from complimentary γ-ray analyses using observations from the *Fermi* γ-ray space telescope and the H.E.S.S. air Čerenkov telescope. Thus, we find no evidence of previously suggested processes for the modification of γ-ray spectra other than that of absorption by pair production alone.

Key words: diffuse radiation – galaxies: luminosity function, mass function – Sun: infrared

1. INTRODUCTION

We have previously employed a *fully empirical* approach to calculating the intergalactic background light (IBL) to wavelengths up to 5 μm by using observational data from deep galaxy surveys (Stecker et al. 2012 (hereafter SMS12); and Scully et al. 2014 (hereafter SMS14)); for a similar approach, see also Helgason & Kashlinsky (2012) and Khaire & Srianand (2015). Here we extend our previous results from SMS12 and SMS14, determining both the IBL at longer wavelengths out to 850 μm and the subsequent γ-ray opacity of the universe out to multi-TeV energies. The spectra of astrophysical sources of such high-energy γ-rays are being studied by ground-based air Čerenkov telescopes and linked air Čerenkov telescope arrays.

We accomplish the goals of this paper by using very recent deep galaxy survey data at far-infrared wavelengths where galaxy emission is produced by dust re-radiation rather than starlight. We also include the γ-ray opacity from photons of the 2.7 K cosmic background radiation (CBR). This enables us to extend our calculations of the γ-ray opacity of the universe to energies much greater than a TeV.

Observations at wavelengths greater than 24 μm, have been covered by the Multiband Imaging Photometer on the *Spitzer* space telescope, now being dramatically advanced by the availability of data from the Photoconductor Array Camera and Spectrometer and Spectral Photometric Imaging Receiver (SPIRE) instruments on the *Herschel* space telescope, the *Planck* space telescope, and by ground-based observations from the *Atacama Large Millimeter Array* (*ALMA*) and observations from the *Balloon-borne Large Aperture Submillimeter Telescope* (*BLAST*). By using only empirical data rather that modeling, our approach is, by definition, *model independent*. We use published luminosity functions (LFs) and interpolations of luminosity densities (LDs) between observed wavebands, observations from high-redshift galaxy surveys being now sufficient for this purpose.

Most past approaches to determining the IBL and its present-day spectral energy distribution (SED), referred to as the "extralgalactic background light (EBL)," require assumptions about how the galaxy LFs evolve (e.g., Malkan & Stecker 1998, 2001; Kneiske, et al. 2002; Stecker et al. 2006 (SMS06); Franceschini et al. 2008; Finke et al. 2010; Kneiske & Dole 2010). Other approaches make use of semi-analytic models that require various assumptions regarding galaxy evolution, stellar population synthesis modeling, or star formation rates the properties of and dust attenuation, particularly for redshifts greater than 1 (e.g., Salamon & Stecker 1998; Gilmore et al. 2009; Domínguez et al. 2011; Somerville et al. 2012; Inoue et al. 2013; Driver et al. 2016). In contrast, our observationally based approach is superior to model-based methods, since it enables a determination of both the IBL *and its observational uncertainties*. This is because we use observationally determined errors. Approaches that rely on modeling cannot determine such uncertainties.

Observational studies of blazar γ-ray spectra have also been used to probe the IBL (Ackermann et al. 2012; Abramowski et al. 2013; Biteau & Williams 2015) through its opacity effect caused by electron–positron pair production. This approach was originally suggested by Stecker et al. (1992) when the infrared EBL was unknown. Our present method of determining the expected γ-ray opacity of the universe by first using observational data to determine the IBL and then calculating its effect on γ-ray spectra of extragalactic sources complements the technique of using direct γ-ray observations. This is because the latter approach requires a thorough knowledge of the intrinsic (unabsorbed) emission spectra of the γ-ray sources. This requirement introduces unavoidable uncertainties.

Our final results give the γ-ray opacity as a function of energy and redshift to within a 68% confidence band that is

based on observational data. This opacity is solely caused by pair-production interactions of IBL photons with extragalactic γ-rays. Thus, a direct comparison of this effect with γ-ray spectra of extragalactic sources enables an assessment of possible additional spectral modifications. One such possible spectral modification has been suggested to be caused by secondary γ-ray production from cosmic-ray interactions along the line of sight to the source (Essey & Kusenko 2014). Another such modification might be caused by photon–axion oscillations during propagation from the source to the Earth (e.g., De Angelis et al. 2007; Meyer & Horns 2013).

In Section 2 we give the details of our calculations of upper and lower limits on IR galaxy LDs for wavelengths between 5 and 850 μm as a function of redshift, paying particular attention to the effects of the emission spectra of polycyclic aromatic hydrocarbons (PAHs). In Section 3 we calculate the $z = 0$ EBL based on the results from Section 2 and compare it with both other work and observational limits. In Section 4 we compute the resulting opacity of the universe to γ-rays out to a redshift of z = 5, including the total opacity from $\gamma + \gamma \rightarrow e^+ + e^-$ interactions with both IBL and thermal CBR photons. In our conclusion section, Section 5, we compare our results with those obtained by other methods in some of the papers mentioned above. We also discuss the implications of our results.

2. CALCULATING THE INFRARED IBL

We have previously calculated the IBL as a function of redshift in the far-ultraviolet to near-infrared range, based purely on data from deep galaxy surveys (SMS12; SMS14). Here we use similar methods to extend the calculation into the mid- and far-infrared IBL out to a wavelength of 850 μm.

2.1. Determining the LDs from Empirical LFs

In our previous work the observationally tolerated ranges of photon densities were determined from the LDs, ρ_{L_ν}, themselves, with errors provided by the various authors at wavelengths ranging from the far-UV to the 5 μm wavelength in the near-IR. The LDs are computed by integrating fits to the observationally determined luminosity functions:

$$\rho_{L_\nu} = \int_{L_{\rm min}}^{L_{\rm max}} dL_\nu \, L_\nu \Phi(L_\nu; z). \quad (1)$$

Cases where authors did not directly compute the LDs were excluded because properly estimating their error requires knowledge of the covariance of the errors in the fit parameters of the LFs and also knowledge of any observational biases. To provide comprehensive redshift coverage of the LDs, SMS12 and SMS14 made use of continuum colors between the wavelength bands to fill in any gaps.

At wavelengths greater than 5 μm very few studies provide determinations of LDs directly, as most authors are more concerned with calculating the *total* IR density, integrated over all wavelengths. This is because the total IR density is an observable that is correlated with the star formation rate. Therefore, in this paper, we used observer-given analytic fits to the LFs at various wavelengths. When those fits were not provided, we ourselves fit the observed infrared galaxy LFs at various wavelengths and redshifts, and then use Equation (1) to obtain the LDs.

Galaxy LFs typically have characteristic shapes that are flatter at lower luminosities but fall off more steeply at the highest luminosities. However, at wavelengths greater than 5 μm the Schechter function, commonly used at optical wavelengths, does not provide a good fit to the observed LFs, as its exponential decrease falls off too quickly at the bright end compared with the measured LFs. Most observers instead fit their LFs to a broken power-law function that describes the data better (e.g., Marchetti et al. 2016). The transition region between the power law that holds at low luminosities and that holds at high luminosities is usually referred to as the *knee* of the LF. The luminosity at the knee is usually designated as L_*. Most of the luminosity density from an LF is produced by galaxies with luminosities in the vicinity of the knee; much fainter galaxies do not contribute much to the LD and the much brighter ones are quite rare. Thus, it is critical to determine the location of the knee in order to estimate the LDs with any accuracy.

For the cases where we were required to determine our own fits, we chose a double power-law fitting function of the form

$$\Phi(L) = \frac{c}{L_*\left(\left(\frac{L}{L_*}\right)^a + \left(\frac{L}{L_*}\right)^b\right)}. \quad (2)$$

Here, the parameters a and b are the indices of the power-law fits in the low-luminosity and high-luminosity ranges, respectively. The overall normalization of the LF is given by the parameter c, which has the dimension of luminosity per Mpc^3 dex. To compute the LDs, we integrate Equation (1) over the galaxy luminosities between 4×10^7 $L_\odot$ and 10^{14} $L_\odot$.

In order to accurately compute the errors in the LDs as derived from the fit parameters, which is essential for our calculation, we must do so in a way that includes terms involving the off-diagonal elements of the error matrix of the fits so as to account for covariance. In cases where the authors provided there own fits, we have therefore re-derived the fits of the LFs to generate the error matrix, retaining the same choice of fitting function and fixed parameters, if given.

Our goal, as in SMS12 and SMS14, was to compute the observationally tolerated ranges of LDs. This requires that we represent the error on these quantities as best we can. The statistical error is determined by properly propagating the fit parameter errors accounting for covariance, lest we overestimate the error. To compute the total error on each LD, we further added in quadrature an additional systematic error that accounts for cosmic variance. We compute cosmic variance based on the field sizes of the individual studies. For the *AKARI Wide Field IR Survey Explorer (WISE)* and GOODS fields, this value is typically of the order of 10%. In determining the LDs, for consistency, all observational LFs are scaled to a Hubble parameter of $h = 0.7$.

Our new additions to our observationally determined LDs extend our coverage of rest frame galaxy photon production from the near-IR to 850 μm in the far-IR, with enough determinations at each wavelength band to span the redshift range $0 \leqslant z \leqslant 2$–3. Using published results derived from observations by the *Spitzer* and *Herschel* space telescopes, sufficient redshift coverage was found for wavelength bands of 8, 12, 15, 24, 35, 60, 90, and 250 μm.

There were two cases where we were required to combine LFs from different observational studies in order to provide enough coverage to discriminate the location of L_* particularly

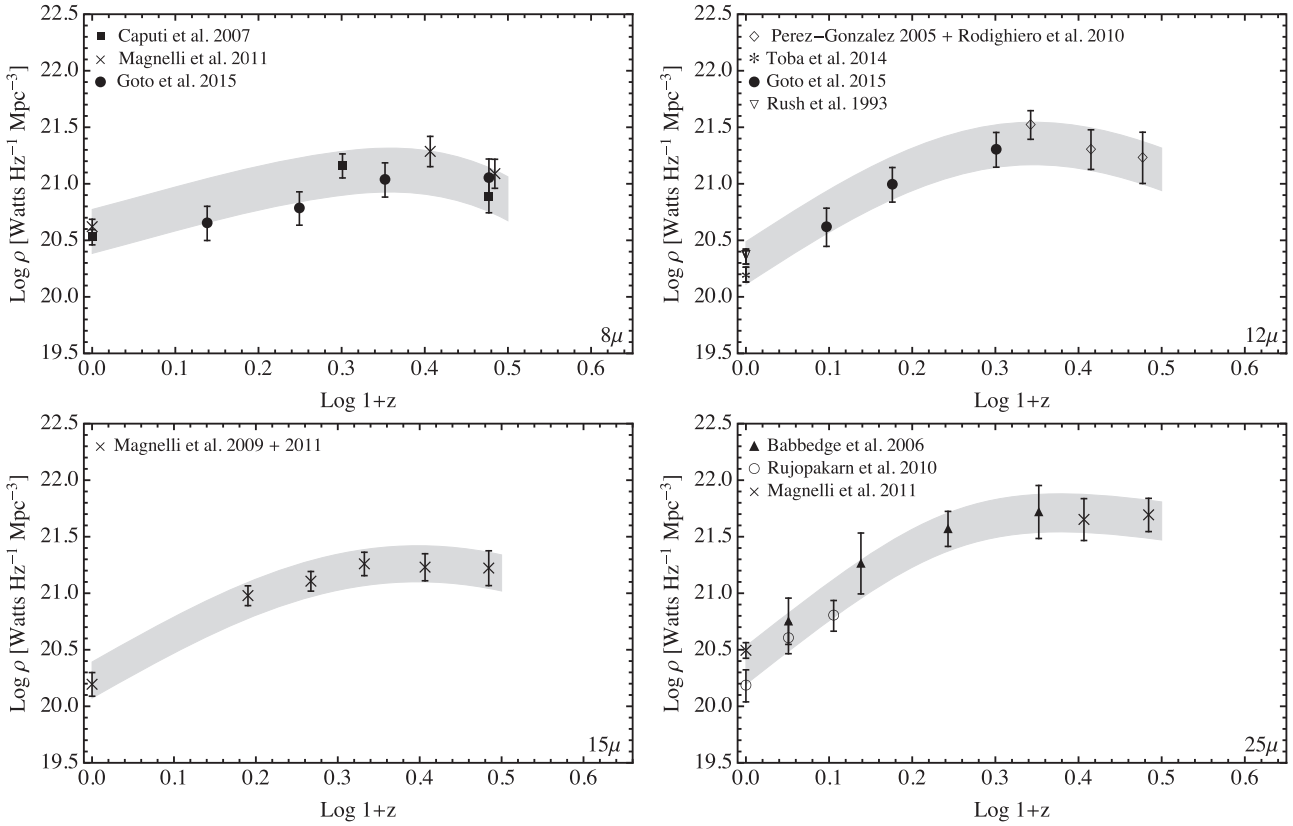

Figure 1. Luminosity densities for the 8, 12, 15, and 24 μm wavebands. Data are from several sources. Some *Spitzer* data from all four wavebands are from Rodighiero et al. (2010). *AKARI* 8 and 12 μm data are from Goto et al. (2015), and *Spitzer* data at 8 μm are from Huang et al. (2007) and Caputi et al. (2007). *Spitzer* data at 8 and 24 μm are from Babbedge et al. (2006). *Spitzer* data at 15 μm are from Le Floc'h et al. (2005). *Spitzer* data at 24 μm are from Pérez-González et al. (2005). The gray shading represents the 68% confidence bands (see text).

for redshifts greater than 1. At 12 μm we combined the results of Pérez-González et al. (2005) and Rodighiero et al. (2010) to compute LDs in redshift bins centered on redshifts of 1.2, 1.6, and 2.0. In order to achieve sufficient redshift coverage at 90 μm we combined some of the higher redshift 100 μm data from Lapi et al. (2011) with that of the 90 μm data from Gruppioni et al. (2013). This gains us additional coverage at redshifts of 1.4, 2.2, and 3.0.

At 160, 350, 500, and 850 μm, LF data only exists for the very nearby redshifts. We therefore assumed that their redshift evolution closely follows that of the 250 μm band (Lapi et al. 2011; Marchetti et al. 2016). We use local LDs calculated in those bands as a normalization to this evolution. This assumption is justified because the emission in this wavelength region is dominated by warm dust. At 160 μm we used the local LF given be Patel et al. (2013). At 350 and 500 μm, we used the combined local LF data of Marchetti et al. (2016) from *Herschel*/SPIRE, the *Herschel*/SPIRE estimate of Vaccari et al. (2010), and the *Planck* satellite data from Negrello et al. (2013). At 850 μm, we computed the local LD from the LF provided by Negrello et al. (2013). Figures 1 and 2 show the resulting derived values for $\rho_{L_\lambda}(z)$ and their errors together with the observationally determined $\pm 1\sigma$ confidence bands for the 8, 12, 15, 24 μm bands and those of 35, 60, 90, and 250 μm, respectively.

Our calculations of LDs at mid-IR to far-IR wavelengths presented here is an extension of the work done in SMS12 and SMS14. Thus, the results given in those papers for wavelengths less than 5 μm is almost unchanged from the results presented here. However, we have updated the far-UV calculations to include the more recent work from Bouwens et al. (2015) for LDs in the redshift range of 4 to 7. Even though the shape of the far-UV band can affect other bands when filling in for redshift gaps using colors, the overall calculation yields results that are qualitatively the same as those presented in SMS12 and SMS14, as the newer data do not significantly change the general trend.

In order to place 68% upper and lower limits by using observational data on ρ_{L_ν} we make as few assumptions about the luminosity density evolution as possible. In SMS12 and SMS14 we utilized a robust rational fitting function in the form of a broken power law dependent on $(1 + z)$ in order to generate the confidence bands. We take the 68% confidence ranges of these fits in each waveband as the $\pm 1\sigma$ confidence bands for the LDs. At redshifts beyond the redshift at the peak of star formation, the LDs decline with redshift. In accord with recent studies of the evolution of rest frame LFs in the UV that trace the star formation rate (Finkelstein et al. 2015), we conservatively assume upper and lower limit power-law functions in redshift to represent the rate of this decline as the highest redshifts. In the upper limit case, we assume a decline proportional to $(1 + z)^{-2}$. In the lower limit case, we adopt a steeper decline proportional to $(1 + z)^{-4}$. These assumptions have almost no impact on the derivation of the opacity confidence bands that we determined. Figures 1 and 2 show our results for LDs as a function of redshift at various wavelengths.

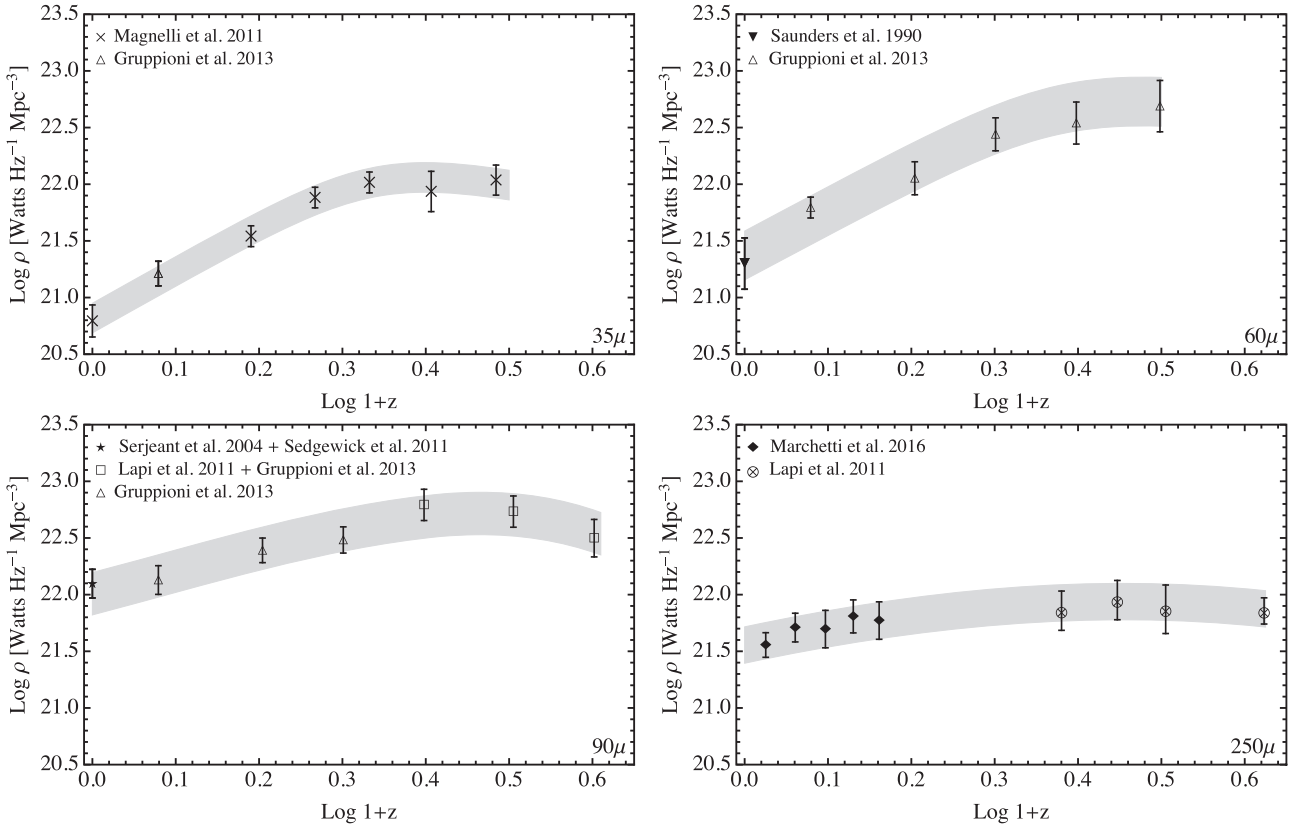

Figure 2. Luminosity densities for the 35, 60, 90, and 250 μm wavebands.The gray shading represents the 68% confidence bands. *Herschel* data at 35, 60, and 90 μm are from Gruppioni et al. (2013). Also, 100 μm data from Lapi et al. (2011) are plotted on the 90 μm graph. *Herschel* data at 250 μm are from Eales et al. (2010), Dye et al. (2010), and Smith et al. (2012, see the text).

2.2. Taking Account of PAH Emission

At wavelengths greater than ~20 μm, the LDs between the bands can be determined by smoothly interpolating between our observationally based LDs at specific wavelengths, since the spectral energy distributions (SEDs) from galaxies in this wavelength range are smooth modified blackbody spectra produced by dust re-radiation. However, in the 5–20 μm range, the situation is more complex.

In star-forming galaxies, the spectra between 7 and 13 μm are dominated primarily by PAH emission. These PAH molecules are found in very small dust grains in intergalactic media. They absorb the UV photons emitted by hot young *O* and *B* stars and reemit them in molecular emission bands in the mid-IR. They are thus a strong signature of active star formation in galaxies (Peeters et al. 2004). In this regard, we note that luminous star forming galaxies at higher redshift have more prominent PAH emission features. The importance of PAH features in the mid-IR at redshifts $0.5 \leqslant z \leqslant 2.5$ has been shown by Lagache et al. (2004).

The average SED of nearby star-forming galaxies (from Spoon et al. 2007, see also Smith et al. 2007) is shown in Figure 3 normalized to our best-fit low-redshift LD confidence band. One can see that there is a relative "valley" between 9 and 11 μm. A simple direct interpolation between our 8 and 12 μm bands would therefore obtain an incorrectly high value for the LD in this wavelength range. Since we do not have wavelength coverage in this regime, we take this feature into account by lowering our interpolated LDs by a factor of 3 for the upper limit and a factor of 5 for the lower limit at 10 μm.

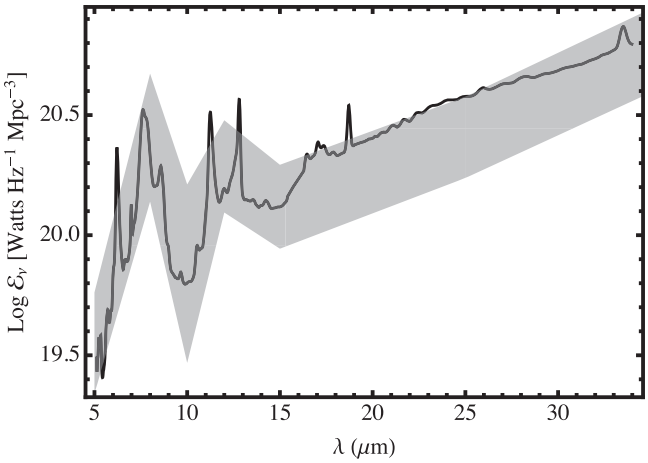

Figure 3. Average low-redshift galaxy SED at MIR wavelengths based on the Class 1C SED of Spoon et al. (2007) normalized to our low-redshift LDs from Figures 1 and 2, as indicated by the shaded region.

The factor of 5 is chosen as a lower limit based on the difference between the peak at 8 μm and the depth of the valley near 10 μm from the SED. For the upper limit, we relax the depth of this feature because, while star forming galaxies make up the bulk of the IBL, contributions from other galaxy types have a less pronounced PAH feature. Since, at high redshifts, PAH emission correlates with the star formation rate (Shipley et al. 2016), we assume that our relative PAH shape factors of 3 and 5 coevolve with redshift.

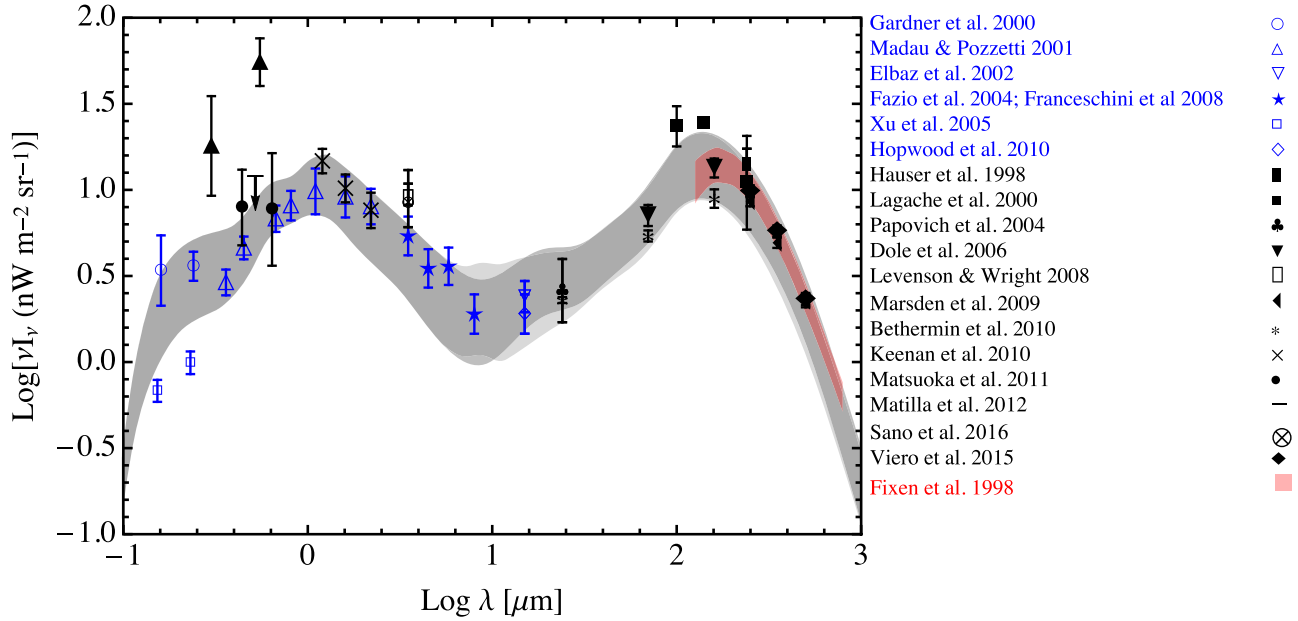

Figure 4. Our spectral energy distribution of the EBL together with empirical data based on our mid-IR LDs and far-IR LDs and the results of SMS12 and SMS14. The light shaded area between ~10 μm and ~30 μm indicates the maximum effect of the PAH bands (see Section 2.2). The lower limits from galaxy counts are shown in blue; direct measurements and extrapolations from galaxy counts in the mid-IR are shown in black. References for the empirical data before 2012 are given by Lagache et al. (2004) and Dwek & Krennrich (2013). A 3.5 μm point is from Sano et al. (2016). The red shaded area is based on the *COBE–FIRAS* results of Fixsen et al. (1998) with limits described by modified blackbody spectra.

3. THE EXTRAGALACTIC BACKGROUND LIGHT

At wavelengths above ~100 μm, the FIRAS and DIRBE instruments onboard the *Cosmic Background Explorer* (*COBE*) have measured the EBL (Fixsen et al. 1998; Lagache et al. 1999). This diffuse background has now been in large part resolved by recent galaxy count studies using the *Herschel* telescope (Berta et al. 2010; Béthermin et al. 2012; Viero et al. 2015) along with ground-based studies using ALMA (Fujimoto et al. 2016) and BLAST (Marsden et al. 2011). These more recent studies strongly support the *COBE* results.

However, there are no direct measurements of the EBL in the infrared range below ~100 μm owing to the predominance of the foreground radiation of Zodiacal light from interplanetary dust re-radiation. The flux of Zodiacal light is approximately two orders of magnitude larger than the EBL flux (Spiesman et al. 1995). In this region, only lower limits obtained from galaxy counts exist.

Using our calculations of the LDs in the mid-IR and far-IR as a function of wavelength, we have constructed a 68% confidence band for the SED of the cosmic diffuse infrared background light (the IBL at $z = 0$). Figure 4 shows our new results, combined with our previous results at shorter wavelengths, taken from SMS12 and SMS14. The light shaded band shows the maximum effect of PAH emission. It can be seen that taking account of the details of the PAH spectrum does not significantly affect our EBL results. Figure 4 also shows the observational lower limits on the EBL obtained from galaxy counts (in blue), extrapolations of mid-IR galaxy counts from *Spitzer*, and direct measurements (in black).

4. THE OPTICAL DEPTH FROM $\gamma + \gamma \rightarrow e^+ + e^-$ INTERACTIONS WITH IBL AND 2.7 K CBR PHOTONS

The co-moving radiation energy density for wavelength λ at redshift z, $u_\nu(z)$, where $\nu = c/\lambda$, is the time integral of the co-moving luminosity density $\rho_\nu(z)$,

$$u_\nu(z) = \int_z^{z_{\max}} dz'\, \rho_{\nu'}(z') \frac{dt}{dz}(z'), \tag{3}$$

where $\nu' = \nu(1 + z')/(1 + z)$, $z_{\max}$ is the redshift corresponding to initial galaxy formation (Salamon & Stecker 1998), and

$$\frac{dt}{dz}(z) = [H_0(1 + z)\sqrt{\Omega_\Lambda + \Omega_m(1 + z)^3}]^{-1}, \tag{4}$$

with $\Omega_\Lambda = 0.72$ and $\Omega_m = 0.28$.

The upper and lower limits on our co-moving energy densities, derived using Equation (3), are shown in Figures 5 and 6.

In calculating the γ-ray opacities we use the relations for the photon energy, $\epsilon_\nu = h\nu$, and the photon density, $n_\nu = \rho_\nu/\epsilon$.

The cross section for photon–photon annihilation to electron-positron pairs was first calculated by Breit & Wheeler (1934) as a solid result of quantum electrodynamics. The threshold for this interaction follows from the Lorentz invariance of the square of the four-momentum vector. This reduces to the square of the threshold energy in the c.m.s., s, that is necessary to produce twice the electron rest mass:

$$s = 2\epsilon E_\gamma(1 - \cos\theta) = 4m_e^2. \tag{5}$$

The Lorentz invariant quantity given by s has been determined to hold to better than one part in 10^{15} (Stecker & Glashow 2001; Jacobson et al. 2004).

The optical depth for γ-rays caused by electron–positron pair production interactions with photons of the stellar radiation

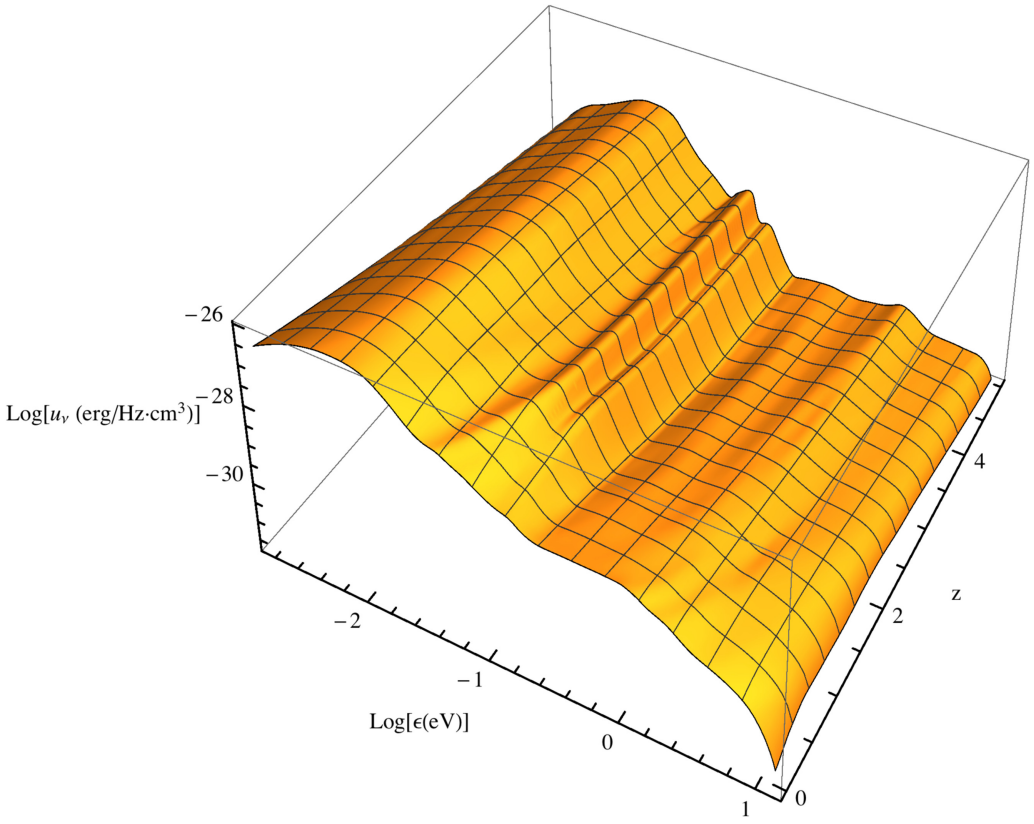

Figure 5. Upper limit envelope on the co-moving energy density as a function of energy and redshift.

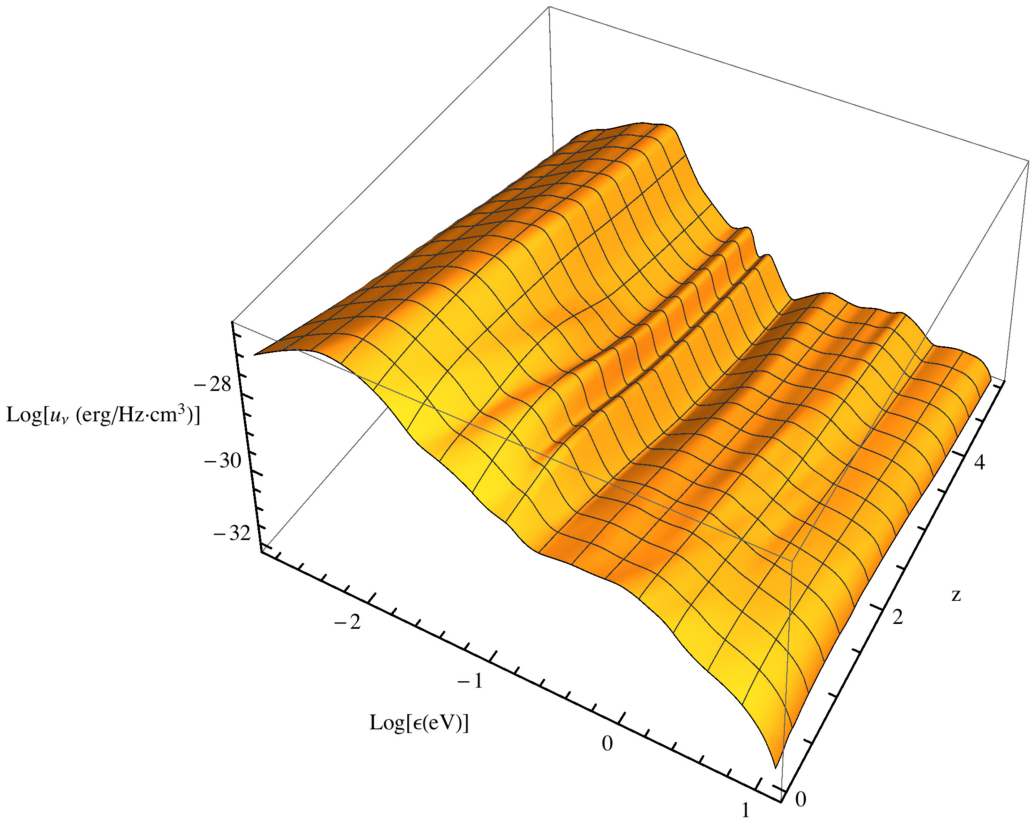

Figure 6. Lower limit envelope on the co-moving energy density as a function of energy and redshift.

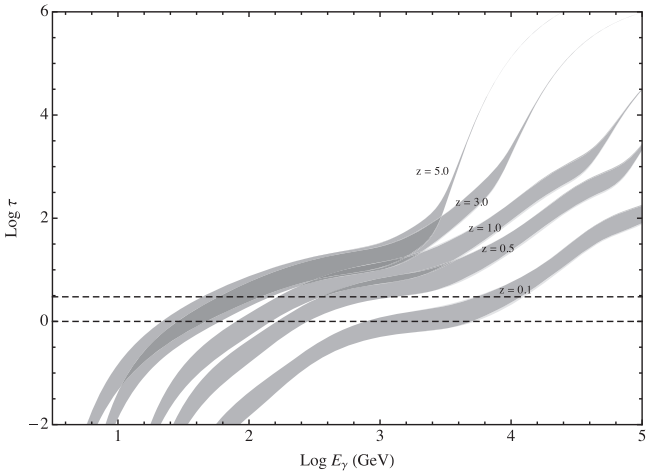

Figure 7. Optical depth of the universe from the IBL and the CBR as well as the total optical depth as a function of energy, given for redshifts of 0.1, 0.5, 1, 3, and 5. It can be seen that the contribution to the optical depth from the IBL dominates at lower γ-ray energies and redshifts and that from the CBR photons dominates at the higher energies and redshifts. The optical depth from CBR photons is an exact function of energy as given by Equation (8) and therefore the confidence band is becomes a thin line. The dashed lines indicate the opacities $\tau = 1$ and $\tau = 3$.

background is given by

$$\tau(E_0, z_e) = c\int_0^{z_e} dz\,\frac{dt}{dz}\int_0^2 dx\,\frac{x}{2}\int_0^\infty d\nu(1+z)^3 \times\left[\frac{u_\nu(z)}{h\nu}\right]\sigma_{\gamma\gamma}[s = 2E_0 hc/\lambda x(1+z)], \quad (6)$$

where $u_\nu(z)$ is the co-moving energy density of the photon field (Stecker et al. 1992).

In Equations (5) and (6), E_0 is the observed γ-ray energy at redshift zero, λ is the wavelength at redshift z, z_e is the redshift of the γ-ray source at emission, $x = (1 - \cos\theta)$, with θ being the angle between the γ-ray and the soft background photon, and the pair production cross section $\sigma_{\gamma\gamma}$ is zero for center-of-mass energy $\sqrt{s} < 2m_e c^2$, with m_e being the electron mass. Above this threshold, the pair production cross section is given by

$$\sigma_{\gamma\gamma}(s) = \frac{3}{16}\sigma_T(1-\beta^2)\left[2\beta(\beta^2-2) + (3-\beta^4)\ln\left(\frac{1+\beta}{1-\beta}\right)\right], \quad (7)$$

where σ_T is the Thompson scattering cross section and $\beta = (1 - 4m_e^2c^4/s)^{1/2}$ (Jauch & Rohrlich 1955).

It follows from Equation (5) that the pair-production cross section has a threshold at $\lambda = 4.75\ \mu\text{m} \cdot E_\gamma(\text{TeV})$.

The optical depth of the universe to the CBR is given by

$$\tau_{\text{CBR}} = 5.00\times 10^5\sqrt{\frac{1.11PeV}{E_\gamma}}\int_0^z \frac{dz'(1+z')\,e^{-\left(\frac{1.11PeV}{E_\gamma(1+z')^2}\right)}}{\sqrt{\Omega_\Lambda + \Omega_m(1+z')^3}} \quad (8)$$

(Stecker 1969; SMS06).

Figure 7 shows the 68% confidence opacity bands for interactions with IBL photons given for sources at $z = 0.1$, 0.5, 1, 3, and 5, calculated using the methods described above, along with the opacity produced by interactions of γ-rays with photons of the 2.7 K CBR. Note that at the higher energies and redshifts where the opacity is dominated by interactions with CRB photons, the uncertainty band becomes a very thin line, since the CBR-dominated opacity is exactly determined by Equation (8).

5. DISCUSSION AND CONCLUSIONS

5.1. Comparison with our Previous Backward Evolution Model

Ten years ago we made estimates of the diffuse infrared background when hardly any mid-IR and far-IR LFs had been observationally determined at high redshifts (SMS06). That work was therefore based on the assumptions of a "backward evolution" model. Starting from the well-determined local ($z = 0$) LF at 60 μm, we assumed that the average locally determined transformations between different mid-IR and far-IR wavelengths applied, unchanged, at all redshifts. The luminosity function used was a double power law, similar to that of Equation (2) with the parameters $a = -1.35$, $b = -3.6$, and $L_* = 8.5\times 10^{23}\,\text{W Hz}^{-1}$ at $z = 0$ as determined at 60 μm, which was the wavelength for which the most complete galaxy LF existed. We then assumed that the effect of redshift evolution could be taken into account purely by the evolution of L_*, as described in SMS06.

We have compared the predictions of the SMS06 backwards evolution model with the recently observed IR LFs as used in this paper. If we make relatively small improvements in the assumed LF parameters, the backwards evolution model agrees with the new observations surprisingly well. The data favor a slightly flatter LF, with a low-luminosity slope of $a = 1.25$ and a high-luminosity slope of $b = 3.25$, provided that we compensate by slightly decreasing the normalization of the LF at L_* and $z = 0$ to $3.5\times 10^{-3}\,\text{Mpc}^{-3}\,\text{dex}^{-1}$. We then match the observed LFs at higher redshifts by assuming that L_* increases as $(1+z)^{3.0}$ for $0 < z < 2.0$, with L_* being constant at higher redshifts. In this way, we can obtain a good fit between the backward evolution model and the observational data.

Although this slightly modified backwards evolution reproduces the observed LFs at all redshifts well, there are a few discrepancies, in either direction. The most substantial disagreement is with the 8 μm observations of Huang et al. (2007) at $z = 0.15$. Below the knee of the LF the observed LF the data are up to 0.3 dex higher than the LF of our backwards evolution model. On the other hand, our best-fitting model overpredicts the 15 μm LFs by up to 0.25 dex at luminosities above the knee as compared with the data of Le Floc'h et al. (2005), Pozzi et al. (2004), and Rodighiero et al. (2010). The likely explanation of both of these discrepancies is that our previously proposed simple model SEDs are based on average 12 μm luminosities as derived from the 60 μm observations. Therefore, they do not include the strong contributions from the PAH bands (See Section 2.2). Thus our SEDs will overpredict the dust continuum on either side of the PAH bump feature as shown in Figure 3. Correspondingly, if we lower the normalization to better fit the shorter and longer wavelengths, we under-estimate the broadband fluxes at 8 μm rest wavelength.

Of course, our new observationally based calculation presented in this paper avoids the problems of backward evolution models, since here we use directly observed LFs at 8,

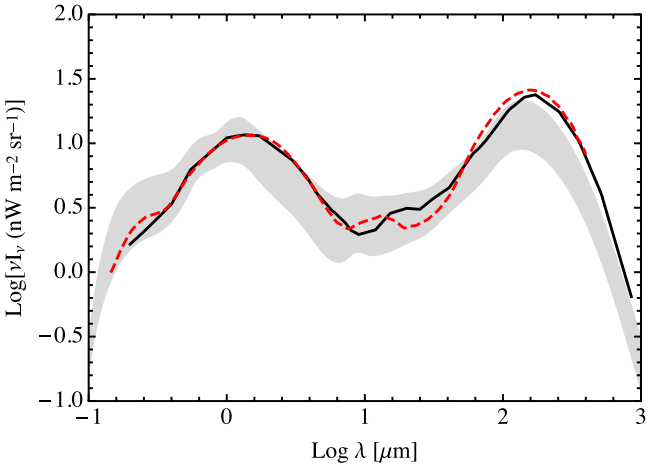

Figure 8. Comparison of our confidence band with the models of Franceschini et al. (2008, solid black line) and Domínguez et al. (2011, red dashed line).

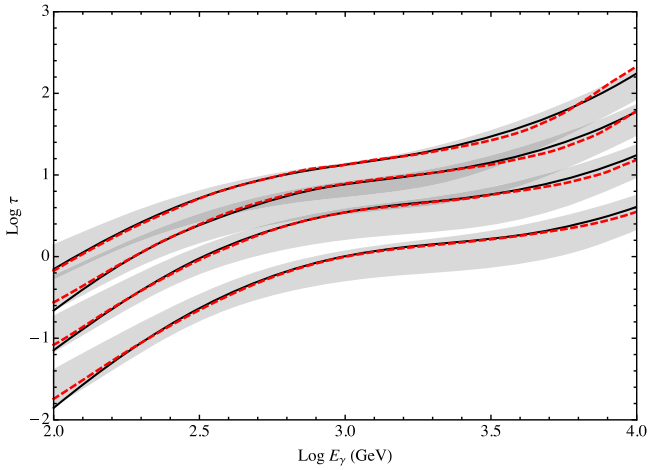

Figure 9. Comparison of our opacity results with those obtained by the models of Franceschini et al. (2008, solid black line) and Domínguez et al. (2011, red dashed line).

15, and 24 μm. These data include the effect of the PAH emission features and show their significance.

5.2. Our Present Results and Comparison with Other Work

Figure 8 shows our 68% confidence band computed for the $z = 0$ IBL (EBL) along with EBL SEDs obtained from the models of Franceschini et al. (2008) and Domínguez et al. (2011). Figure 9 shows our 68% opacity bands for $z = 0.1$, 0.5, 1, 3, and 5, in comparison with the opacity curves of Franceschini et al. (2008), Domínguez et al. (2011). We note that Franceschini et al. (2008) used data only up to 8 μm that were available at the time and did not include a PAH component in their model. The model of Domínguez et al. (2011) assumes a redshift evolution at redshifts greater than ∼1 that follows the evolution in the *K* band given by Cirasuolo et al. (2010).

5.3. Conclusion

In our previous papers (SMS12 and SMS14), we presented observationally based results for the IBL as a function of wavelength and redshift for wavelengths below of 5 μm. Based on those results, we computed the γ-ray opacity of the universe caused by electron–positron pair production up to a γ-ray energy of $1.6/(1 + z)$ TeV. In this paper, we have extended our determinations of the IBL within 68% confidence bands. This determination defines upper and lower limits on the IBL to longer wavelengths that extend to 850 μm. Our model-independent results are based on observationally derived LFs from recent galaxy survey data from both local and high-redshift surveys. These data include results from *Spitzer*, *Herschel*, and *Planck*. We then use these results to calculate the opacity of the universe to γ-rays out to PeV energies. In doing so, we also take account of the redshift dependence of interactions of γ-rays with photons of the 2.7 K CBR (Stecker 1969), since the opacity from interactions with CBR photons dominates over that from interactions with IBL photons at the higher γ-ray energies and redshifts.

In Figure 10, we give an energy-redshift plot showing the highest-energy photons from extragalactic sources as a function of redshifts as determined from *Fermi* data (Abdo et al. 2010) plotted with our 68% confidence band for $\tau = 1$.

Our direct results on the IBL are consistent with those from complimentary γ-ray analyses using observations from the

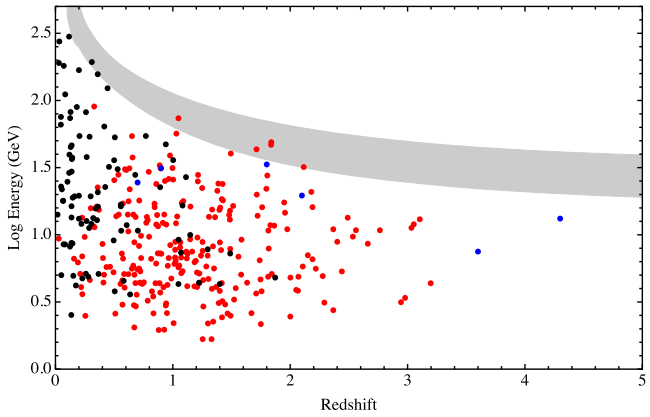

Figure 10. A $\tau = 1$ energy-redshift plot (Fazio & Stecker 1970) showing our uncertainty band results compared with the *Fermi* plot of their highest energy photons from FSRQs (red), BL Lacs (black), and GRBs (blue) vs. redshift (from Abdo et al. 2010).

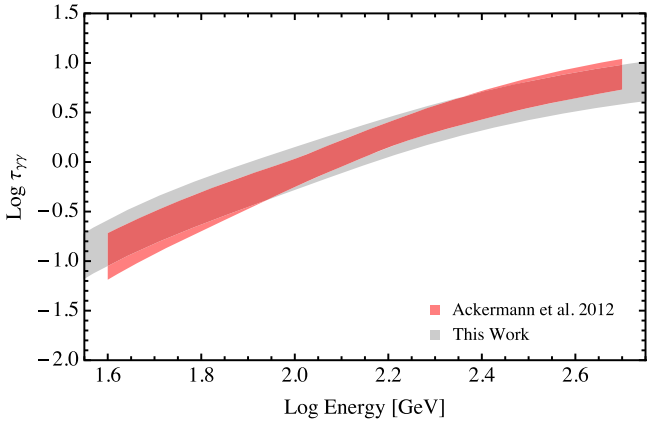

Figure 11. Comparison of our results for $z = 1$ with those obtained from an analysis of blazar γ-ray spectra (Ackermann et al. 2012).

Fermi-LAT γ-ray space telescope and the H.E.S.S. air Čerenkov telescope. Figure 11 indicates how well our opacity results for $z = 1$ overlap with those obtained by the *Fermi* collaboration (Ackermann et al. 2012). Our results are also compatible with those obtained from higher-energy

γ-ray observations using H.E.S.S. (Abramowski et al. 2013). This overlap of results from two completely different methods strengthens confidence that both techniques are indeed complimentary and supports the concept that the spectra of cosmic γ-ray sources can be used to probe the IBL (Stecker et al. 1992).

Thus, we find no evidence for modifications of γ-ray spectra by processes other than absorption by pair production, either by cosmic-ray interactions along the line of sight to the source (Essey & Kusenko 2014) or line-of-sight photon–axion oscillations during propagation (e.g., De Angelis et al. 2007; Meyer & Horns 2013). In this regard, we note that the *Fermi* Collaboration has very recently searched for irregularities in the γ-ray spectrum of NGC 1275 that would be caused by photon–axion oscillations and reported negative results (Ajello et al. 2016).

We conclude that modification of the high-energy γ-ray spectra of extragalactic sources occurs dominantly by pair production interactions of these γ-rays with photons of the IBL. They therefore support the concept of using the future Čerenkov Telescope Array instruments to probe the cosmic background radiation fields at infrared wavelengths. This method can be used in conjunction with future deep galaxy survey observations using the near-infrared and mid-infrared instruments onboard the *James Webb Space Telescope*.

REFERENCES

Abdo, A., Ackermann, M., Ajello, M., et al. 2010, ApJ, 723, 1082
Abramowski, A., Acero, F., Aharonian, F., et al. 2013, A&A, 550, A4
Ackermann, M., Ajello, M., Allafort, A., et al. 2012, Sci, 338, 1190
Ajello, M., Albert, A., Anderson, B., et al. 2016, PhRvL, 116, 161101
Babbedge, T. S. R., Rowan-Robinson, M., Vaccari, M., et al. 2006, MNRAS, 370, 1159
Béthermin, M., Le Floc'h, E., Ilbert, O., et al. 2012, A&A, 542, A58
Berta, S., Magnelli, B., Lutz, D., et al. 2010, A&A, 518, L30
Bouwens, R. J., Illingworth, G. D., & Oesch, P. A. 2015, ApJ, 803, 34
Biteau, J., & Williams, D. A. 2015, ApJ, 812, 60
Breit, G., & Wheeler, J. A. 1934, PhRv, 46, 1087
Caputi, K. I., Lagache, G., Yan, L., et al. 2007, ApJ, 660, 97
Cirasuolo, M., McLure, R. J., Dunlop, J. S., et al. 2010, MNRAS, 401, 1166
De Angelis, A., Roncadelli, M., & Mansutti, O. 2007, PhRvD, 76, 121301
Domínguez, A., Primack, J. R., Rosario, D. J., et al. 2011, MNRAS, 410, 2556
Driver, S. P., Andrews, S. K., Davies, L. J., et al. 2016, arXiv:1605.01523
Dye, S., Dunne, L., Eales, S., et al. 2010, A&A, 518, L10
Dwek, E., & Krennrich, F. 2013, APh, 43, 112
Eales, S., Raymond, G., Roseboom, I. G., et al. 2010, A&A, 518, L23
Essey, W., & Kusenko, A. 2014, APh, 57, 30
Fazio, G. G., & Stecker, F. W. 1970, Natur, 226, 135
Finke, J. D., Razzaque, S., & Dermer, C. D. 2010, ApJ, 712, 238
Finkelstein, S. L., Ryan, R. E., Jr., Papovich, C., et al. 2015, ApJ, 810, 71
Fixsen, D. J., Dwek, E., Mather, J. C., Bennett, C. L., & Shafer, R. A. 1998, ApJ, 508, 123
Franceschini, A., Rodighiero, G., & Vaccari, M. 2008, A&A, 487, 837
Fujimoto, S., Ouchi, M., Ono, Y., et al. 2016, ApJS, 1, 222
Gilmore, R. C., Madau, P., Primack, J. R., et al. 2009, MNRAS, 399, 1694
Goto, T., Oi, N., Ohyama, Y., et al. 2015, MNRAS, 452, 1684
Gruppioni, C., Pozzi, F., Rodighiero, G., et al. 2013, MNRAS, 432, 23
Huang, J.-S., Ashby, M. L. N., Barmby, P., et al. 2007, ApJ, 664, 840
Helgason, K., & Kashlinsky, A. 2012, ApJ, 758, L13
Inoue, Y., Inoue, S., Kobayashi, M. A. R., et al. 2013, ApJ, 768, 197
Jacobson, T., Liberati, S., Mattingly, D., & Stecker, F. W. 2004, PhRvL, 93, 021101
Jauch, J. M., & Rohrlich, F. 1955, The Theory of Photons and Electrons (Cambridge, MA: Addison-Wesley)
Khaire, V., & Srianand, R. 2015, ApJ, 805, 33
Kneiske, T. M., & Dole, H. 2010, A&A, 515, A19
Kneiske, T. M., Mannheim, K., & Hartmann, D. H. 2002, A&A, 386, 1
Lagache, G., Abergel, A., Boulanger, F., et al. 1999, A&A, 344, 322
Lagache, G., Dole, H., Puget, J.-L., et al. 2004, ApJS, 154, 112
Lapi, A., González-Nuevo, J., Fan, L., et al. 2011, ApJ, 742, 24
Le Floc'h, E., Papovich, C., Dole, H., et al. 2005, ApJ, 632, 169
Malkan, M. A., & Stecker, F. W. 1998, ApJ, 496, 13
Malkan, M. A., & Stecker, F. W. 2001, ApJ, 555, 641
Marchetti, L., Vaccari, M., Franceschini, A., et al. 2016, MNRAS, 456, 1999
Marsden, G., Chapin, E. L., Halpern, M., et al. 2011, MNRAS, 417, 1192
Meyer, M., & Horns, D. 2013, PhRvD, 87, 035027
Negrello, M., Clemens, M., Gonzalez-Nuevo, J., et al. 2013, MNRAS, 429, 1309
Patel, H., Clemens, D. L., Vaccari, M., et al. 2013, MNRAS, 428, 291
Peeters, E., Spoon, H. W. W., & Tielens, A. G. G. M. 2004, ApJ, 613, 986
Pérez-González, P. G., Pablo, G., Rieke, G. H., et al. 2005, ApJ, 630, 82
Pozzi, F., Gruppioni, C., Oliver, S., et al. 2004, ApJ, 609, 122
Rodighiero, G., Vaccari, M., Franceschini, A., et al. 2010, A&A, 518, A8
Salamon, M. H., & Stecker, F. W. 1998, ApJ, 493, 547
Sano, K., Kawara, K., Matsuura, S., et al. 2016, ApJ, 818, 72
Scully, S. T., Malkan, M. A., & Stecker, F. W. 2014, ApJ, 784, 138 (SMS14)
Shipley, H. V., Heath, V., Papovich, C., et al. 2016, ApJ, 818, 60
Smith, D. J. B., Dunne, L., da Cunha, E., et al. 2012, MNRAS, 427, 703
Smith, J. D. T., Draine, B. T., Dale, D. A., et al. 2007, ApJ, 656, 770
Somerville, R. S., Gilmore, R. C., Primack, J. R., & Domínguez, A. 2012, MNRAS, 423, 1992
Spiesman, W. J., Hauser, M. G., Kelsall, T., et al. 1995, ApJ, 442, 662
Spoon, H. W. W., Marshall, J. A., Houck, J. R., et al. 2007, ApJL, 654, L49
Stecker, F. W. 1969, ApJ, 157, 507
Stecker, F. W., De Jager, O. C., & Salamon, M. H. 1992, ApJL, 390, L49
Stecker, F. W., & Glashow, S. L. 2001, APh, 16, 97
Stecker, F. W., Malkan, M. A., & Scully, S. T. 2006, ApJ, 648, 774 (SMS06)
Stecker, F. W., Malkan, M. A., & Scully, S. T. 2012, ApJ, 761, 128 (SMS12)
Vaccari, M., Marchetti, L., Franceschini, A., et al. 2010, A&A, 518, L20
Viero, M. P., Moncelsi, L., Quadri, R. F., et al. 2015, ApJL, 809, L22

The Astrophysical Journal, 863:112 (1pp), 2018 August 10 https://doi.org/10.3847/1538-4357/aad563

Erratum: "An Empirical Determination of the Intergalactic Background Light from UV to FIR Wavelengths Using FIR Deep Galaxy Surveys and the Gamma-Ray Opacity of the Universe" (2016, ApJ, 827, 6)

Floyd W. Stecker[1,2], Sean T. Scully[3], and Matthew A. Malkan[2]
[1] Astrophysics Science Division, NASA/Goddard Space Flight Center, Greenbelt, MD 20771, USA; Floyd.W.Stecker@nasa.gov
[2] Department of Physics and Astronomy, University of California, Los Angeles, CA 90095-1547, USA; scullyst@jmu.edu
[3] Department of Physics, James Madison University, Harrisonburg, VA 22807, USA; malkan@astro.ucla.edu
Received 2018 July 13; published 2018 August 14

In the published article, Figure 9, referenced in Section 5.2, shows the results for $z = 0.1$, 0.3, 0.6, and 1.0 in order to compare with other results. The results in Figure 9 are not $z = 0.1$, 0.5, 1, 3, 5 as erroneously stated in the text.

ORCID iDs

Floyd W. Stecker https://orcid.org/0000-0002-1515-100X Matthew A. Malkan https://orcid.org/0000-0001-6919-1237